CORA Cork Open Research Archive
Cartlann Taighde Oscailte Chorcaí

Title	Synthesis of novel quinine analogs and evaluation of their effects on Trypanosoma cruzi
Authors	Ceole, Ligia F.;Gandhi, Hirenkumar;Villamizar, Luz H.;Soares, Maurilio J.;O'Sullivan, Timothy P.
Publication date	2018-02-01
Original Citation	Ceole, L. F., Gandhi, H., Villamizar, L. H., Soares, M. J. and O'Sullivan, T. P. (2018) 'Synthesis of novel quinine analogs and evaluation of their effects on Trypanosoma cruzi', Future Medicinal Chemistry, 10(4), pp. 391-408. doi: 10.4155/fmc-2017-0184
Type of publication	Article (peer-reviewed)
Link to publisher's version	https://www.future-science.com/doi/abs/10.4155/fmc-2017-0184 - 10.4155/fmc-2017-0184
Rights	© 2018 Newlands Press. For full bibliographic citation, please refer to the version available at www.future-science.com
Download date	2026-11-03 15:37:31
Item downloaded from	https://hdl.handle.net/10468/7168

UCC
University College Cork, Ireland
Coláiste na hOllscoile Corcaigh

The published manuscript is available at Future Medicincal Chemistry via:

https://www.future-science.com/doi/abs/10.4155/fmc-2017-0184

Synthesis of novel quinine analogues and evaluation of their effects on *Trypanosoma cruzi*

Ligia F. Ceole[1#], Hirenkumar Gandhi[2,3#], Luz H. Villamizar[4], Maurilio J. Soares[1], Timothy P. O'Sullivan[2,3,5*]

[1]Laboratory of Cell Biology, Carlos Chagas Institute/Fiocruz, Curitiba, PR, Brazil

[2]School of Chemistry, University College Cork, Cork, Ireland.

[3]Analytical and Biological Chemistry Research Facility, University College Cork, Cork, Ireland.

[4]Laboratory of Molecular Biology of Trypanosomatids, Carlos Chagas Institute/ Fiocruz, Curitiba, PR, Brazil.

[5]School of Pharmacy, University College Cork, Cork, Ireland.[1]

Abstract

Background: Chagas disease is a tropical disease caused by the hemoflagellate protozoan *Trypanosoma cruzi*. There is no vaccine for Chagas disease and available drugs (e.g. benznidazole) are effective only during the acute phase, displaying a variable curative activity in the established chronic form of the disease. New leads with high efficacy and better toxicity profiles are urgently required. **Methodology:** A library of novel quinine derivatives was synthesised using Heck chemistry and evaluated against the various developmental forms of *T. cruzi*. **Conclusions:** Several novel quinine analogues with trypanocidal activity have been identified with the *para*-nitro-substituted derivative displaying a submicromolar IC_{50} which is 83 times lower than quinine and three times lower than benznidazole. Transmission electron microscopy analysis demonstrated that these compounds induced a marked vacuolisation of the kinetoplast of intracellular amastigotes and cell-derived trypomastigotes.

Keywords

Chagas disease, quinine, Heck coupling, *Trypanosoma cruzi*, trypanocides, kinetoplast vacuolisation, ultrastructure

[1] # LFC and HG contributed equally to this work.

1. Introduction

Chagas disease is a tropical neglected disease caused by the hemoflagellate protozoan *Trypanosoma cruzi* [1]. An estimated 6 million to 7 million people are infected worldwide, mostly in Latin America. Chagas disease has spread to other continents over the last century driven by movement of people and international trade.

There is currently no vaccine for Chagas disease and the available drugs (nifurtimox and benznidazole) were developed more than four decades ago [2]. Both are effective only if given soon after infection at the onset of the acute phase. The efficacy of both diminishes, however, the longer a person has been infected [3]. These compounds do not completely reduce the parasite load in the bloodstream and may display serious side effects [4]. The associated side effects, including anorexia, vomiting, peripheral polyneuropathy and allergic dermopathy, can in some cases lead to treatment discontinuation [5]. Therefore, there is an on-going global effort to find new natural and synthetic compounds with high efficacy and less adverse side effects.

Quinine is the major alkaloid found in the bark of various species of *Cinchona* (*Rubiaceae*) trees [6]. It was the first effective treatment for malaria until the 1940s, when other drugs with fewer side effects (such as chloroquine and artemisinin) replaced it [7]. More recently, it has been demonstrated that quinine possesses potent schizonticidal action against intra-erythrocytic malaria parasites [8]. Merschjohann and co-workers investigated the effect of 34 alkaloids on the growth of *Trypanosoma brucei* and *T. congolense in vitro*. Quinine, berbamine, berberine, cinchonidine, cinchonine, emetine, ergotamine, quinidine and sanguinarine showed trypanocidal activities with ED_{50} values below 10 µM [9]. Ruiz-Mesia *et al.* tested several *Cinchona* alkaloids isolated from *Remijia peruviana* against *T. cruzi* and found that only quinine displayed moderate trypanocidal activity [10]. A similar observation was also made by Sepúlveda-Boza and Cassels [11].

Given the well-known activity of quinine derivatives against the apicomplexan *Plasmodium*, we wondered if similar analogues might be effective against the pathogenic protozoan *T. cruzi*. Three main types of modification have been traditionally made to the quinine scaffold, namely modification of the quinolone/quinuclidine ring, substitution of the hydroxyl group or manipulation of the stereochemical configuration [12, 13]. It has been demonstrated that both the hydroxyl group and quinolone ring are

essential for antimalarial activity [14]. More recently, the terminal alkene in quinine has been identified as a versatile synthetic handle, particularly in the development of novel asymmetric catalysts [15-19]. The manipulation of this fragment in medicinal chemistry is less common. Significantly, Dinio *et al.* found that the introduction of aryl substituents was associated with higher potency against both quinine-sensitive and quinine-resistant strains of *Plasmodium* [20]. Furthermore, Bhattacharjee *et al*. have proposed a binding model which suggests that the quinine vinyl group may be important for activity [21].

In view of these results, we sought to employ a similar strategy against *T. cruzi*. Modification of the alkene by way of Heck chemistry should be relatively straight forward [22]. A library of quinine analogues generated in this fashion should provide insights into the importance of the alkene functionality and highlight possible structure activity relationships.

2 Experimental Protocols

2.1 Reagents and data collection

MTT (Thiazolyl Blue Tetrazolium Bromide) was purchased from Invitrogen (Carlsbad, CA, USA). Benznidazole, DAPI (4′,6-Diamidine-2′-phenylindole dihydrochloride), DMSO (dimethyl sulfoxide) and DMEM (Dulbecco's Modified Eagle's Medium) were purchased from Sigma-Aldrich (St. Louis, MO, USA). Fetal bovine serum was purchased from Thermo Fisher Scientific (Carlbad, CA, USA). All solvents were purified and dried using standard methods prior to use. Commercially available reagents were used without further purification. The reactions were monitored by thin layer chromatography (TLC), using MERCK pre-coated silica gel 60-F_{254} aluminium plates. Visualisation of spots on TLC plates was done by UV light. Column chromatography with 230-400 mesh silica gel was used as the purification method. A gradient combination of dichloromethane and methanol was used as eluent. ^{1}H-NMR spectra were recorded on an Avance NMR instrument operated at 400 MHz. ^{13}C-NMR spectra were recorded on an Avance NMR instrument operated at 100 MHz. All spectra were recorded at room temperature (approximately 20 °C) in deuterated chloroform ($CDCl_3$). Chemical shifts values were reported in ppm with TMS as an internal reference and *J* values were given in Hertz. The following abbreviation were used for ^{1}H-NMR spectra

to indicate the signal multiplicity: s (singlet), d (doublet), dd (double doublet), ddd (double double doublet), m (multiplet). HRMS were determined with Waters LCT Premier Time of Flight spectrometer in electrospray ionisation (ESI) mode using 50% water/acetonitrile containing 0.1% formic acid as eluent and samples were made up in acetonitrile.

*2.2 General synthetic procedure for compounds **2**-**5** and **8**-**11***

Quinine (**1**) (250 mg, 0.77 mmol), palladium(II) acetate (8.7 mg, 0.039 mmol), and triphenylphosphine or tri(*o*-tolyl)phosphine (0.077 mmol, 10 mol%) were added to a sealed, oven-dried tube under an inert atmosphere of nitrogen. The aryl halide (1.54 mmol, 2.0 equiv.) in degassed, anhydrous toluene (1.5 mL) was added to the reaction tube *via* syringe, followed by triethylamine or tributylamine (1.54 mmol, 2.0 equiv.). The reaction mixture was stirred at 111 °C until the reaction had reached completion. The reaction mixture was allowed to cool to room temperature and the solvent was removed *in vacuo* to furnish a reddish coloured semi-solid material. The crude solid was dissolved in dichloromethane (10 mL), filtered through a cotton plug and the resulting filtrate was concentrated *in vacuo* at 50-55 °C for 3 hours to fully remove the excess base. The residue was purified using silica gel column chromatography using a gradient solvent system of dichloromethane and MeOH (98:2 to 85:15). The fractions containing the product were combined and the solvent was removed *in vacuo* to afford the product as an amorphous solid.

*2.3 11-(Phenyl)-quinine (**2**)*[20]

Off-white solid, yield 89%; ^{1}H-NMR (400MHz, $CDCl_3$): δ 8.65 (1H, d, *J* = 4.4 Hz), 7.76 (1H, d, *J* = 9.2 Hz), 7.61 (1H, d, *J* = 4.4 Hz), 7.10 (5H, m), 6.99 (2H, m), 6.58 (1H, m), 6.32 (1H, d, *J* = 15.8 Hz), 5.79 (1H, dd, *J1* = 7.6 Hz, *J2* = 15.8 Hz), 4.46 (1H, OH), 3.70 (3H, s), 3.55 (1H, m), 3.42 (1H, m), 3.17 (2H, m), 3.03 (1H, m), 2.86 (1H, m), 2.20 (2H, m), 1.88 (2H, m), 1.38 (1H, m); ^{13}C-NMR (100MHz, $CDCl_3$) : δ 158.7, 147.0, 143.8, 143.6, 135.7, 133.02, 131.4, 128.6, 126.2, 122.8, 119.1, 100.1, 66.1, 60.4, 58.7, 55.7, 44.5, 36.8, 27.6, 24.2, 18.8; HRMS (ESI): *m/z* mass calc for $C_{26}H_{29}N_2O_3$ ($M+H^+$) 401.2229, Found 401.2233.

*2.4 11-(Bis-3,5-trifluoromethyl)phenyl-quinine (**3**)*

Off-white solid, yield 86%; ^{1}H-NMR (300MHz, $CDCl_3$): δ 8.70 (1H, d, *J* = 4.5 Hz), 8.01 (1H, d, *J* = 9.2 Hz), 7.66 (2H, s), 7.40 (1H, dd, *J1* = 2.6 Hz, *J2* = 9.3 Hz), 7.26-7.31 (5H, m), 7.20 (1H, m), 6.40 (1H, d, *J* = 16.1 Hz), 6.10 (1H, dd, *J1* = 7.9 Hz, *J2* = 16.1 Hz), 5.29 (1H, s), 4.0 (3H, s), 3.45 (1H, m), 3.33 (2H, m), 2.97 (2H, m), 2.54 (1H, m), 1.77 (1H, m), 1.67 (2H, m), 1.62 (2H, m); ^{13}C-NMR (100MHz, $CDCl_3$): δ 157.8, 147.7, 144.4, 139.4, 138.0, 132.1, 132.0, 131.8, 128.5, 128.4, 127.6, 126.7, 125.8, 120.4, 118.4, 101.5, 72.2, 60.4, 57.3, 55.7, 43.1, 39.9, 28.2, 27.6, 22.3; HRMS (ESI): *m/z* mass calc for $C_{26}H_{27}N_2O_2F_6$ ($M+H^+$) 537.1977 Found 537.1970.

*2.5 11-(3,4,5-Trifluorophenyl)-quinine (**4**)*

Off-white solid, yield 71%; ^{1}H-NMR (400MHz, $CDCl_3$): δ 8.69 (1H, *d*, J = 4.5 Hz), 7.71 (1H, d, *J* = 9.2 Hz), 7.68 (1H, d, *J* = 4.5 Hz), 7.01 (1H, dd, *J1* = 2.4 Hz, *J2* = 9.2 Hz), 6.94 (1H, d, *J* = 2.3 Hz), 6.75 (2H, m), 6.50 (1H, d, *J* = 16.1 Hz), 6.23 (1H, d, *J* = 15.8 Hz), 5.81 (1H, dd, *J1* = 7.6 Hz, *J2* = 15.8 Hz), 4.55 (1H, OH), 3.66 (3H, s), 3.56 (1H, m), 3.41 (1H, m), 3.16 (1H, m), 3.03 (1H, m), 2.85 (1H, m), 2.30 (1H, m), 2.16 (2H, m), 1.90 (1H, m), 1.37 (1H, m);^{13}C-NMR (100MHz, $CDCl_3$): δ 158.3, 152.5, 150.1, 147.0, 143.7, 143.6, 139.4, 131.4, 130.7, 130.2, 125.3, 122.3, 118.9, 110.2, 110.0, 99.9, 66.1, 60.3, 57.6, 55.4, 44.3, 36.9, 27.5, 24.3, 21.1, 18.5; HRMS (ESI): *m/z* mass calc for $C_{26}H_{26}N_2O_2F_3$ ($M+H^+$) 455.1946 Found 455.1951.

*2.6 11-(2,4,6-Trifluorophenyl)-quinine (**5**)*

Off-white solid, yield 69%; ^{1}H-NMR (300MHz, $CDCl_3$): δ 8.69 (1H, d, *J* = 4.5 Hz), 8.0 (1H, d, *J* = 9.2 Hz), 7.51 (1H, d, *J* = 4.5 Hz), 7.35 (1H, dd, *J1* = 2.6 Hz, *J2* = 9.3 Hz), 7.27 (1H, d, *J* = 2.7 Hz), 6.84 (2H, m), 6.20 (1H, d, *J* = 15.8 Hz), 6.08 (1H, dd, *J1* = 7.9 Hz, *J2* = 15.8 Hz), 5.55 (1H, d, *J* = 4.2 Hz), 3.92 (3H, s), 3.45 (1H, m), 3.18 (2H, m), 2.69 (2H, m), 2.43 (1H, m), 1.87 (2H, m), 1.63 (1H, m), 1.53 (2H, m); ^{13}C-NMR (100MHz, $CDCl_3$): δ 164.2, 162.2, 157.8, 147.7, 147.4, 144.4, 136.2, 131.7, 127.5, 126.7, 121.5, 118.3, 109.8, 109.6, 101.4, 72.2, 60.3, 57.4, 55.7, 43.1, 39.6, 28.2, 27.6, 22.1; HRMS (ESI): *m/z* mass calc for $C_{26}H_{26}N_2O_2F_3$ ($M+H^+$) 455.1946 Found 455.1942.

*2.7 11-(4-Nitrophenyl)-quinine (**8**)*

White solid, yield 82%; ^{1}H-NMR (400MHz, $CDCl_3$): δ 8.69 (1H, d, *J* = 4.5 Hz), 8.05 (2H, m), 7.71 (1H, d, *J* = 9.2 Hz), 7.66 (1H, d, *J* = 4.5 Hz), 7.29 (2H, m), 6.99 (1H, dd,

J1 = 2.6 Hz, *J2* = 9.2 Hz), 6.93 (1H, d, *J* = 2.3 Hz), 6.43 (1H, d, *J* = 16.1 Hz), 6.10 (1H, dd, *J1* = 7.9 Hz, *J2* = 16.1 Hz), 4.50 (1H, m), 3.66 (3H, s), 3.54 (1H, m), 3.33 (2H, m), 3.13 (2H, m), 3.0 (1H, m), 2.88 (1H, m), 2.29 (1H, m), 1.88 (2H, m), 1.40 (2H, m); ^{13}C-NMR (100MHz, $CDCl_3$): δ 158.1, 147.1, 147.0, 144.1, 143.6, 142.2, 133.6, 131.4, 130.8, 126.8, 125.3, 124.0, 122.0, 118.8, 99.9, 66.4, 60.4, 56.9, 55.4, 44.1, 37.6, 27.5, 24.6, 18.7; HRMS (ESI): *m/z* mass calc for $C_{26}H_{27}N_3O_4$ ($M+H^+$) 446.2080 Found 446.2080.

*2.8 11-(4-Methoxyphenyl)-quinine (**9**)*[20]

Off-white solid, yield 68%; ^{1}H-NMR (400MHz, $CDCl_3$): δ 8.68 (1H, d, *J* = 4.5 Hz), 7.71 (1H, d, *J* = 9.3 Hz), 7.69 (1H, d, *J* = 4.6 Hz), 7.16 (3H, m), 7.07 (1H, d, *J* = 8.6 Hz), 6.99 (1H, dd, *J1* = 2.3 Hz, *J2* = 9.2 Hz), 6.92 (1H, d, *J* = 2.3 Hz), 6.71 (1H, d, *J* = 8.7 Hz), 6.49 (1H, d, *J* = 15.8 Hz), 6.33 (1H, dd, *J1* = 7.6 Hz, *J2* = 15.8 Hz), 5.69 (1H, m), 4.55 (1H, m), 3.73 (3H, s), 3.65 (3H, s), 3.63 (1H, m), 3.55 (1H, m), 3.41 (1H, m), 3.16 (2H, m), 3.0 (1H, m), 2.85 (1H, m), 2.29 (1H, m), 2.14 (2H, m), 1.90 (2H, m), 1.40 (2H, m); ^{13}C-NMR (100MHz, $CDCl_3$): δ 158.3, 147.0, 143.9, 143.7, 132.8, 132.2, 131.3, 128.6, 127.4, 126.2, 122.3, 119.0, 114.0, 99.8, 66.1, 60.4, 57.6, 55.8, 55.3, 44.3, 37.0, 27.6, 24.4, 18.5; HRMS (ESI): *m/z* mass calc for $C_{26}H_{30}N_2O_3$ ($M+H^+$) 431.2335 Found 431.2326.

*2.9 11-(4-Cyanophenyl)-quinine (**10**)*

Off-white solid, yield 63%; ^{1}H-NMR (400MHz, $CDCl_3$): δ 8.63 (1H, d, *J* = 4.48 Hz), 7.70 (1H, d, *J* = 9.27 Hz), 7.59 (1H, d, *J* = 4.52), 7.42 (2H, m), 7.18 (2H, m), 6.98 (2H, m), 6.47 (1H, d, *J* = 15.8 Hz), 6.33 (1H, dd, *J1* = 7.65 Hz, *J2* = 15.78 Hz), 5.93 (1H, m), 4.51 (1H, m), 3.63 (3H, s), 3.51 (1H, m), 3.47 (1H, m), 3.13 (2H, m), 3.0 (1H, m), 2.85 (1H, m), 2.29 (1H, m), 2.13 (2H, m), 1.85 (2H, m), 1.37 (2H, m); ^{13}C-NMR (100MHz, $CDCl_3$): δ 158.3, 147.0, 143.9, 143.8, 143.6, 140.04, 132.4, 132.1, 131.5, 131.4, 126.8, 122.2, 118.9, 111.4, 99.94, 66.1, 60.4, 57.6, 55.4, 44.1, 37.1, 27.5, 24.4, 18.6; HRMS (ESI): *m/z* mass calc for $C_{27}H_{27}N_3O_2$ ($M+H^+$) 426.2182 Found 426.2178.

*2.10 11-(4-Methylphenyl)-quinine (**11**)*[20]

White solid, yield 87%; ^{1}H-NMR (400MHz, $CDCl_3$): δ 8.71 (1H, d, *J* = 4.51 Hz), 7.80 (1H, d, *J* = 9.12 Hz), 7.70 (1H, d, *J* = 4.48 Hz), 7.45 (1H, d, *J* = 8.31 Hz), 7.25 (2H, m), 7.10 (2H, m), 6.52 (1H, s), 6.42 (1H, d, *J* = 15.8 Hz), 5.97 (1H, dd, *J1* = 7.70 Hz, *J2* =

15.8 Hz), 4.55 (1H, m), 3.77 (3H, s), 3.59 (1H, m), 3.47 (1H, m), 3.18 (1H, m), 3.1 (1H, m), 2.94 (3H, m), 2.26 (3H, s), 1.90 (2H, m), 1.37 (2H, m); ^{13}C-NMR (100MHz, $CDCl_3$): δ 158.5, 147.2, 144.0, 143.7, 139.1, 131.7, 131.6, 130.9, 126.4, 125.6, 122.3, 119.0, 100.1, 66.1, 60.4, 57.6, 55.8, 55.6, 47.6, 44.3, 37.1, 29.7, 27.7, 27.5, 24.4, 20.1, 18.6; HRMS (ESI): *m/z* mass calc for $C_{27}H_{31}N_2O_2$ ($M+H^+$) 415.2386 Found 415.2386.

*2.11 Synthetic procedure for (9S,8S)-9-amino-(9-deoxymethyl)-epiquinine (**6**)*[19]

Quinine (**1**) (2g, 6.16 mmol) and triphenylphosphine (2 g, 7.62 mmol) were charged to a three neck 100 mL RBF followed by 50 mL of dry tetrahydrofuran under a nitrogen atmosphere. The reaction was cooled to -5 °C and stirred until the solution turned clear. Diisopropyl azadicarboxylate (DIAD) (1.5 g, 7.42 mmol) was added dropwise *via* syringe at -5 °C. The reaction was stirred for 30 minutes before diphenylphosphoryl azide (DPPA) (2.1 g, 7.63 mmol) was added dropwise *via* syringe at -5 °C. The reaction mixture was heated to room temperature and stirred for a further 18 hours. The reaction mixture was subsequently stirred at 60 °C for 2 hours. Triphenylphosphine (2.1 g, 8.0 mmol) was added and stirring continued for 4 hours. The reaction mixture was cooled to room temperature and deionised water (2.0 mL) was added before stirring for 18 hours. The solvent was removed *in vacuo* and the remaining aqueous layer was extracted with CH_2Cl_2:2M HCl (1:1, 80 mL). The dichlormethane layer was discarded and the aqueous layer was concentrated *in vacuo*. The crude product was purified *via* recrystallisation from hot methanol (4.0 mL) to afford (9*S*,8*S*)-9-amino-(9-deoxymethyl)-epiquinine hydrochloride as an off-white solid. The salt was basified with saturated sodium bicarbonate solution (20 mL) and extracted with CH_2Cl_2 (3 x 20 mL). Removal of the solvent *in vacuo* furnished (9*S*,8*S*)-9-amino-(9-deoxymethyl)-epiquinine (free base) as a yellow oil in 75% yield.

^{1}H-NMR (300 MHz, CDCl3): δ 8.75 (1H, d, J = 4.55 Hz), 8.04 (1H, d, J = 9.22 Hz), 7.65 (1H, br, s), 7.45 (1H, d, J = 4.48 Hz), 7.39 (1H, dd, J_1 = 2.75 Hz, J_2 = 9.24 Hz), 5.81 (1H, ddd, J_1 = 7.35 Hz, J_2 = 10.25 Hz, J_3 = 17.52 Hz), 4.99 (2H, m), 4.60 (1H, d, J = 10.25 Hz), 3.97 (3H, s), 3.28 (1H, dd, J_1 = 10.25 Hz, J_2 = 13.85 Hz), 3.10 (1H, m), 2.81 (2H, m), 2.28 (1H, m), 1.63 (1H, m), 1.56 (2H, m), 1.44 (1H, m); ^{13}C-NMR (100MHz, CDCl3): δ 157.7, 147.9, 144.8, 141.8, 131.8, 128.8, 121.2, 119.9, 114.3, 102.1, 61.9, 56.4, 55.6, 52.5, 41.0, 39.9, 28.2, 27.6, 26.1; HRMS (ESI): *m/z* mass calc for $C_{20}H_{25}N_3O$ ($M+H^+$) 324.2076 Found 324.2075.

*2.12 Synthetic procedure for 11-phenyl-(9S,8S)-9-amino-(9-deoxymethyl)-epiquinine (**7**)*[19]

(9*S*,8*S*)-9-Amino-(9-deoxymethyl)-epiquinine (**6**) (100 mg, 0.31 mmol), palladium(II) acetate (3.48 mg, 0.0155 mmol), and triphenylphosphine (0.077 mmol, 0.031 mmol) were added to a sealed, oven-dried tube under an inert atmosphere of nitrogen. Iodobenzene (0.62 mmol, 2.0 equiv.) in degassed, anhydrous toluene (1.5 mL) was added to the reaction tube *via* syringe followed by triethylamine (0.62 mmol, 2.0 equiv). The reaction mixture was stirred at 111 °C until the reaction had reached completion after 18 h. The reaction mixture was allowed to cool to room temperature and the solvent was removed *in vacuo* to furnish a reddish coloured semi-solid material. The crude solid was dissolved in dichloromethane (10 mL) and filtered through a cotton plug. The resulting filtrate was concentrated *in vacuo* before extraction with CH_2Cl_2:2M HCl (1:1, 20 mL). The dichloromethane layer was discarded and the aqueous layer was concentrated *in vacuo*. The crude product was purified *via* recrystallisation from hot methanol (3.0 mL) to afford 11-phenyl-(9*S*,8*S*)-9-amino-(9-deoxymethyl)-epiquinine hydrochloride as a yellow solid. The salt was basified with saturated sodium bircarbonate solution (10 mL) and extracted with CH_2Cl_2 (2 x 10 mL). Removal of the solvent *in vacuo* furnished 11-phenyl-(9*S*,8*S*)-9-amino-(9-deoxymethyl)-epiquinine as a yellow solid in 84% yield.

^{1}H-NMR (300MHz, $CDCl_3$): δ 8.77 (1H, d, *J* = 4.52 Hz), 8.04 (1H, d, *J* = 9.22 Hz), 7.51 (1H, d, *J* = 4.32 Hz), 7.40 (1H, dd, *J1* = 2.65 Hz, *J2* = 9.34 Hz), 7.26-7.31 (5H, m), 7.20 (1H, m), 6.40 (1H, d, *J* = 16.1 Hz), 6.18 (1H, dd, *J1* = 7.94 Hz, *J2* = 16.1 Hz), 4.68 (1H, s), 4.0 (3H, s), 3.45 (1H, m), 3.33 (2H, m), 2.97 (2H, m), 2.54 (1H, m), 1.77 (1H, m), 1.67 (2H, m), 1.62 (2H, m); ^{13}C-NMR (100MHz, $CDCl_3$): δ 157.8, 147.9, 144.8, 137.2, 132.6, 132.0, 130.5, 128.6, 127.3, 126.1, 121.4, 119.0, 101.3, 71.7, 61.3, 56.7, 55.8, 52.2, 41.2, 39.0, 27.9, 27.7, 25.9; HRMS (ESI): *m/z* mass calc for $C_{26}H_{29}N_2O_3$ ($M+H^+$) 400.2389 Found 400.2389.

2.13 Vero Cells

Vero cells (ATCC CCL-81) were kept in 75 cm^2 tissue culture flasks at 37 °C in a humidified 5% CO_2 atmosphere with DMEM supplemented with 5% fetal bovine serum. For the weekly seeding, cell monolayers were washed twice with PBS (pH 7.2),

trypsinised and the detached cells were collected by centrifugation for 5 min at 800*g*. The cells were inoculated at $9x10^5$ cells/flask in fresh medium and kept as described above.

2.14 Parasites

Epimastigote forms of *Trypanosoma cruzi*, clone Dm28c, were kept at 28 °C in LIT (Liver Infusion-Tryptose) medium supplemented with 10% inactivated fetal bovine serum, with passages at every three days. Parasites from 72-hour cultures were used for the experiments.

Cell-derived trypomastigotes were obtained from the supernatant of previously infected Vero cell cultures and used for re-infections. Briefly, Vero cells ($1.3x10^6$ cells) and cell-derived trypomastigotes (ratio 1:10) were seeded into 75 cm^2 tissue culture flasks in DMEM medium. After 4 h of incubation, the cultures were washed with DMEM to remove non-internalized parasites and then kept in DMEM at 37 °C in a humidified 5% CO_2 atmosphere. Cell-derived trypomastigotes were collected in the supernatant 96 h post-infection.

2.15 Drug assays on epimastigotes

Three-day-old culture epimastigotes were collected, adjusted to a concentration of $5x10^6$ cells/well in 100 µL LIT medium and seeded into 96 well plates. Different concentrations of the compounds were then added (final concentrations in 200 µL: 3.125, 6.25, 12.5, 25, 50 and 100 µM) and the plates were incubated for 24 h at 28 ºC. Benznidazole (7.81, 15.625, 31.25, 62.5 and 125 µM) was used as a positive control. Cell viability was assessed by the MTT methodology [23]. Briefly, after incubation with the drugs, 50 µL MTT (previously prepared at 10 mg/mL in PBS) was added to each well, with final concentration of 2 mg/mL MTT per well. The plates were wrapped in aluminium foil, incubated for 4 h at 28 °C, centrifuged for 15 min at 500*g* and the supernatant was removed. For cell lysis, 50 µL of a SDS/HCl solution (10% SDS, 0.01 M HCl) was added to each well. After solubilisation, absorbance of the samples was read at 570 nm in an ELISA plate reader (Biotek Model EL800, Winooski, VT, USA). Dose-response curves were obtained with GraphPad Prism software (La Jolla, CA, USA) and the IC_{50}/24 h value (concentration that inhibits culture growth in 50%) was then calculated. Absorbance of untreated cells (negative control) was used as 100% cell viability. The percentage of no-viable cells in each treatment was estimated by

comparison with the negative control. Experiments were made in biological duplicate, each one in technical triplicate.

2.16 Drug assays on intracellular amastigotes and cytotoxicity

Vero cells ($5x10^3$ cells/well) and cell-derived trypomastigotes (ratio 1:20) were seeded into 96-well plates in DMEM medium. After 4 h of incubation, the cultures were washed with DMEM to remove non-internalized parasites and then kept in 300 µL DMEM at 37 °C in a humidified 5% CO_2 atmosphere. After 24 h of incubation, the infected Vero cell cultures with intracellular amastigotes were incubated with DMEM containing different drug concentrations (final concentration ranging from 0.078 to 2000 µM) in a total volume of 200 µL/well. After incubation for additional 24 h the plates were washed with PBS, fixed for 5 minutes with cold methanol and cell nuclei were stained with DAPI (5 µg/mL). Images were obtained with an Operetta imaging system (Perkin Elmer, Waltham, MA, USA) on the DAPI channel, at 20x magnification. About 30-40 fields per well were captured, each field with five stacked images.

It has been shown that Operetta is a reliable methodology for amastigote counting [24]. By using the Operetta Imaging system Harmony Software (Perkin Elmer, USA) the following parameters were defined: (*a*) percentage of infected Vero cells, (*b*) number of amastigotes per host cell, and (*c*) the Infectivity Index (II = *a* x *b*). The IC_{50}/24 h value was then estimated from II, by comparing with the control (100% viability). Dose-response curves were obtained with GraphPad Prism software. For cytotoxicity with the synthetic compounds, the parameter used was the total number of Vero cell nuclei. All experiments were performed in a single biological experiment, in technical sextuplicates. The Selectivity Index was obtained according to the formula: $SI=CC_{50}/IC_{50}$.

2.17 Drug assays on cell-derived trypomastigotes and cytotoxicity

Cell-derived trypomastigotes were collected, adjusted to a concentration of $1x10^7$ cells/well in 100 µL DMEM medium and seeded into 96-well plates. Different concentrations of **9** were then added (final concentrations in 200 µL: 1.562, 3.125, 6.25, 12.5, 25, 50 and 100 µM) and the plates were incubated for 2 h at 37 ºC (longer incubation times resulted in transformation into the amastigote form). Benznidazole (up to 1000 µM) was used as control. Cell viability was assessed by the MTT methodology,

by incubating with 2 mg/mL MTT for 2 h at 37 ºC. For cell lysis, 50 µL DMSO plus 50 µL of a SDS/HCl solution were added to each well. After solubilisation, absorbance of the samples was read at 570 nm in an ELISA plate reader and the IC_{50}/2 h value was then estimated.

For cytotoxicity, Vero cells ($1.25x10^5$ cells/ml) were seeded in 96-well plates, 100 µl per well, and cultivated for 24 h. Thereafter, different concentrations of **9** were added (final concentrations in 200 µL: 12.5, 25, 50 and 100 µM) and the plates were incubated for 2 h at 37 ºC. Cell viability was assessed by the MTT methodology. Briefly, after incubation with the drugs, 50 µL MTT (previously prepared at 10 mg/mL in PBS) was added to each well, with final concentration of 2 mg/mL MTT per well. The plates were wrapped in aluminium foil, incubated for 2 h at 37 °C. For cell lysis, 50 µL of DMSO was added to each well. After solubilisation, absorbance of the samples was read at 570 nm in an ELISA plate reader. Dose-response curves were obtained with GraphPad Prism software (La Jolla, CA, USA) and the CC_{50}/2 h value was calculated. Absorbance of untreated cells (control) was used as 100% cell viability. Experiments were made in biological duplicate.

2.18 Infectivity assay

Vero cells ($6x10^6$ cells/well) and **9**-treated (IC_{50}/2 h value) trypomastigotes (ratio 1:10) were seeded into 6-well plates in DMEM medium. After 2 h of incubation, the cultures were washed with DMEM to remove non-adherent parasites and then incubated for further 48 h. After this time the cell cultures were fixed for 5 minutes with cold methanol and the cell nuclei were stained with 5 µg/mL DAPI. The percentage of infected Vero cells and the total number of intracellular amastigotes was estimated by counting 2,000 host cells in 05 randomly selected microscopic fields photographed in a Leica DMI6000B fluorescence microscope (20x objective) associated to a Leica AF6000 deconvolution software (Leica Microsystems, Buffalo Grove, IL, USA). The Infectivity Index (II) was calculated as described previously.

2.19 Scanning Electron Microscopy (SEM)

Cell-derived trypomastigotes ($4.5x10^7$/well) were incubated for 2 h with 12.5 µM **9**, washed with PBS and fixed for 2 h with 2.5% glutaraldehyde in 0.1 M cacodylate buffer, pH 7.2. The cells were then adhered for 10 minutes to glass coverslips previously coated with 0.1% poly-L-lysine. The cells were washed in 0.1 M cacodylate

buffer and post-fixed for 5 minutes with 1% osmium tetroxide in this same buffer. After washing in buffer the samples were dehydrated in graded acetone series and dried in a Leica CPD300 critical point drier (Leica Mikrosysteme GmbH, Vienna, Austria). The coverslips were adhered to SEM stubs and coated with 20-nm thick gold layer in a Leica EM ACE200 sputtering device. The cells were then observed in a Jeol JSM6010Plus-LA scanning electron microscope. Untreated trypomastigotes were used as control.

Additionally, Vero cells ($1.25x10^5$/well) and **9**-treated trypomastigotes (ratio 1:10) were seeded into 24-well plates in DMEM medium, each well containing a glass coverslip. The cell cultures were incubated for 2 h, washed with PBS to remove non-adherent parasites and the coverslips were then fixed with glutaraldehyde and processed as above.

2.20 Transmission Electron Microscopy

Infected Vero cells with intracellular amastigotes (24-hour-old cultures) were incubated for 24 h with **1**, **8**, **9** and **11** and then processed for conventional transmission electron microscopy. Briefly, the cell cultures were fixed for 2 h with 2.5% glutaraldehyde in 0.1 M cacodylate buffer pH 7.2, washed in buffer and then post-fixed for 1 h with 1% osmium tetroxide in cacodylate buffer. The samples were dehydrated in graded acetone series and embedded in Embed812 resin (EMS, Hatfield, PA, USA). Ultrathin sections were collected on cupper grids, stained with uranyl acetate and lead citrate and observed under a Jeol 1400Plus transmission electron microscope at 80 kV.

Cell-derived trypomastigotes ($4.5x10^7$/well) were incubated for 2 h with the IC_{50} value of **9** (12.5 µM), washed with PBS, fixed for 2 h with 2.5% glutaraldehyde in cacodylate buffer and processed as above. Furthermore, Vero cells ($6x10^6$ cells/well) and **9**-treated trypomastigotes (ratio 1:10) were seeded into 6-well plates in DMEM medium. The cell cultures were incubated for 2 h, 24 h or 48 h, washed with PBS, and then fixed with glutaraldehyde and processed as above.

3. Results and discussion

3.1 Chemistry

The synthetic route to the compound library is outlined in Figure 1. Based on our previous efforts to develop novel quinine-derived organocatalysts [19], the target

compounds **2** to **11** were synthesized *via* a palladium-catalysed Heck coupling of commercially available quinine and the appropriate aryl halide under a nitrogen atmosphere (Table 1). This Heck chemistry displayed high selectively, with the *trans*-isomer being formed exclusively in each case. Conversion to the Heck product was found to be dependent on the choice of ligand and base, as well as the nature of the aryl halide. Palladium acetate in combination with triphenylphosphine proved generally efficacious, although recourse to tri(*o*-tolyl)phosphine was required in some cases (entries 3, 4). Likewise, while triethylamine was a suitable base for this reaction (entries 1, 9), the higher reaction temperatures afforded by use of tri-*n*-butylamine generally afforded higher yields overall (entries 2-8). In terms of substrate scope, fluorinated aryl halides were found to be less reactive (entries 4, 5). The reactivity suffered further as the number of fluorines on the aryl ring was increased, with pentafluorophenyl iodide failing to react under optimised conditions. Finally, replacement of the hydroxyl with an amine group by way of a Mitsunobu-Staudinger reaction furnished **6** with complete inversion of stereochemistry. The resulting amine derivative was subjected to Heck coupling with phenyl iodide affording **7** in 84% yield as the *trans*-isomer.

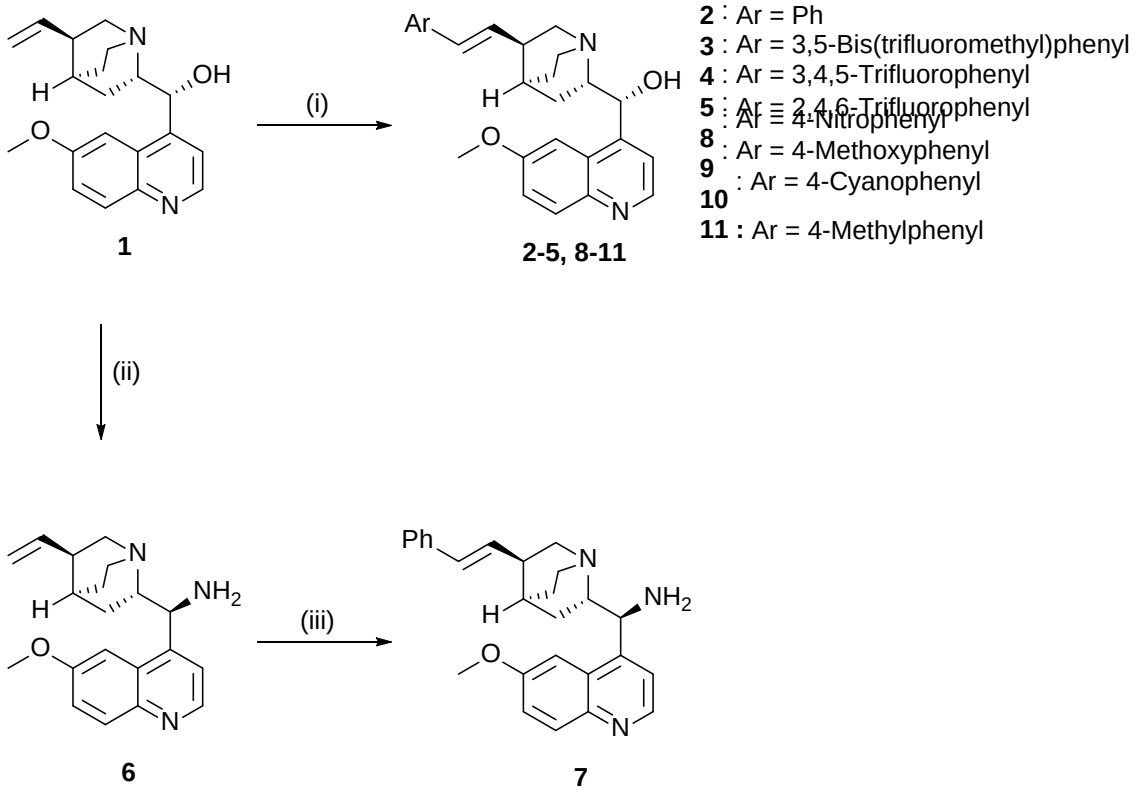
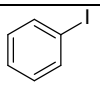
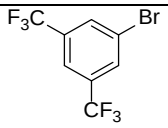
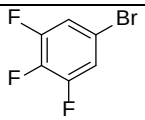
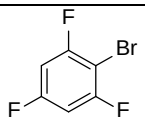
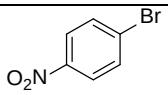
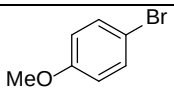
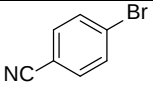
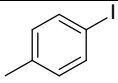


Figure 1. Synthesis of quinine analogues; Reagents and conditions: (i) $Pd(OAc)_2$ (5 mol%), triphenylphosphine or (tri-*o*-tolyl)phosphine (10 mol%), Ar-X (2 equiv.), triethylamine or tributylamine (2 equiv.), toluene, reflux, N_2, 24 h. (ii) DIAD (1.2 equiv.), diphenylphosphorylazide (1.3 equiv.), triphenylphosphine (2.6 equiv.), anhydrous tetrahydrofuran, -10 to 60 °C, 75%. (iii) $Pd(OAc)_2$ (5 mol%), triphenylphosphine (10 mol%), Ph-I (2 equiv.), tributylamine (2 equiv.), toluene, reflux, N_2, 24 h, 84%.

Table 1. Optimised conditions for the synthesis of quinine analogues *via* Heck coupling

Entry	Compound	Ar-X	Ligand	Base	Time	Yield
1	**2**		PPh_3	Et_3N	16 h	89%
2	**3**		PPh_3	*n*-Bu_3N	24 h	86%
3	**4**		P(*o*-tol)$_3$	*n*-Bu_3N	34 h	71%
4	**5**		P(*o*-tol)$_3$	*n*-Bu_3N	34 h	69%
5	**7**		PPh_3	*n*-Bu_3N	18 h	84%
6	**8**		PPh_3	*n*-Bu_3N	18 h	82%
7	**9**		PPh_3	*n*-Bu_3N	18 h	68%
8	**10**		PPh_3	*n*-Bu_3N	18 h	63%
9	**11**		PPh_3	Et_3N	16 h	87%

3.2 Biological evaluation

Compounds **1** to **7** were initially screened against culture epimastigotes, in order to assess their possible trypanocidal activity. The existence of an intracellular epimastigote-like form as an intermediate stage within the mammalian host supports the preliminary screening of trypanocidal compounds on this non-infectious stage of the

parasite [25]. Naturally occurring quinine (**1**) showed very weak activity (IC_{50}/24 h higher than 100 µM) (Table 2, entry 1). On foot of the promising results previously reported by Dinio *et al*., the introduction of an aryl-substituent onto the olefinic side chain was investigated [20]. This modification was accompanied by an increase in potency with phenyl-substituted **2** displaying an IC_{50}/24 h of 31.37 µM (entry 2). This improved activity may be partially rationalised by the increase in lipophilicity associated with the presence of the non-polar phenyl ring (cLogP 4.12 *vs.* 2.51). Extending this logic further, fluorine is often used to modulate the physicochemical properties of drugs, such as lipophilicity or electron density [26]. Fluorinated analogues **3-5** were found to be comparable to **2** (entries 3-5). Compound **3**, which was the most lipophilic derivative (cLog P 5.87) with two trifluoromethyl substituents on the aromatic ring, was the best candidate within this group, with an IC_{50}/24 h of 18.86 ± 3.9 µM (entry 3). We also wished to ascertain whether the secondary alcohol group was a prequisite for activity. Replacing the hydroxyl in quinine with an amine *via* Mitsunobu-Staudinger chemistry afforded **6** which was, unsurprisingly, discovered to be inactive (entry 6). Indeed, culture epimastigotes remained alive in the presence of 100 µM of **6** over six days, when the cultures were then discarded. However, when **6** was subjected to a palladium-mediated coupling with phenyl iodide to furnish **7**, the phenyl-substituted product displayed activity similar to **2** in spite of the absence of the hydroxyl group (entries 7 vs 2).

Table 2. Effect of quinine derivatives (**1** to **11**) and benznidazole (BZ, control drug) on different *T. cruzi* developmental forms (culture epimastigotes and intracellular amastigotes) and host Vero cells, with determination of Inhibitory Concentration 50% (IC_{50}) and cytotoxicity 50% (CC_{50}). SI = Selectivity Index (CC_{50}/IC_{50}).

Entry	Compound	IC_{50} (µM) Epimastigote	IC_{50} (µM) Amastigote	CC_{50} (µM) Vero cell	SI Amastigote	cLog P
1	**1**	>100	80.35	288.46	3.59	2.51
2	**2**	31.37 ± 3.96	7.50	18.46	2.46	4.12
3	**3**	18.86 ± 3.95	15.00	5.19	0.35	5.87
4	**4**	40.29 ± 9.01	5.19	6.35	1.22	4.54

5	**5**	44.28 ± 4.55	17.31	22.50	1.30	4.54
6	**6**	>100	818.18	1365.35	1.67	2.41
7	**7**	35.14 ± 9.64	30.58	20.77	0.68	4.01
8	**8**	55.32 ± 6.36	0.96	10.6	11.04	4.06
9	**9**	11.30 ± 4.21	1.15	7.4	6.43	3.96
10	**10**	63.98 ± 9.68	8.09	11.43	1.41	3.97
11	**11**	40.89 ± 2.28	2.31	7.8	3.38	4.63
12	BZ	59	3.07[a]	3920.00[a]	1276.87[a]	

IC_{50}: inhibitory concentration for 50% of parasites after 24 h

CC_{50}: cytotoxic concentration for 50% of Vero cell cultures after 24 h

SI: selectivity index

BZ: benznidazole

cLog P calculated using Chemaxon Marvinsketch software package.

[a]See ref 27

Since this initial screening had returned some promising results, these compounds were next tested against intracellular amastigotes. The majority were found to active with IC_{50} values ranging from 5 to 31 μM (Table 2, entries 2-5, 7 and Figure 2A-C), apart from quinine (80.35 μM, entry 1) and **6** (818.18 μM, entry 6) in line with earlier results. Notably, all compounds were more active against intracellular amastigotes than culture epimastigotes. The introduction of an aromatic ring was found to be strongly beneficial, with phenyl-substituted **2** being 10-fold more active than quinine (entry 2 vs 1). Similarly, phenyl-substituted **7** was 27 times more effective than amine **2** (entry 7 vs 6). The impact of the substitution pattern on the aromatic ring is apparent when comparing 3,4,5-trifluorinated **4** to 2,4,6-trifluorinated **5**. Despite both compounds being isomers of one another, **4** is over three times more potent than **5**. All of the active compounds showed relatively high cytotoxicity against the host Vero cells (Figure 2D-F). Quinine and **6**, the two inactive compounds, were significantly less cytotoxic. The best Selectivity Index (SI) value was obtained for quinine with an SI of 3.59.

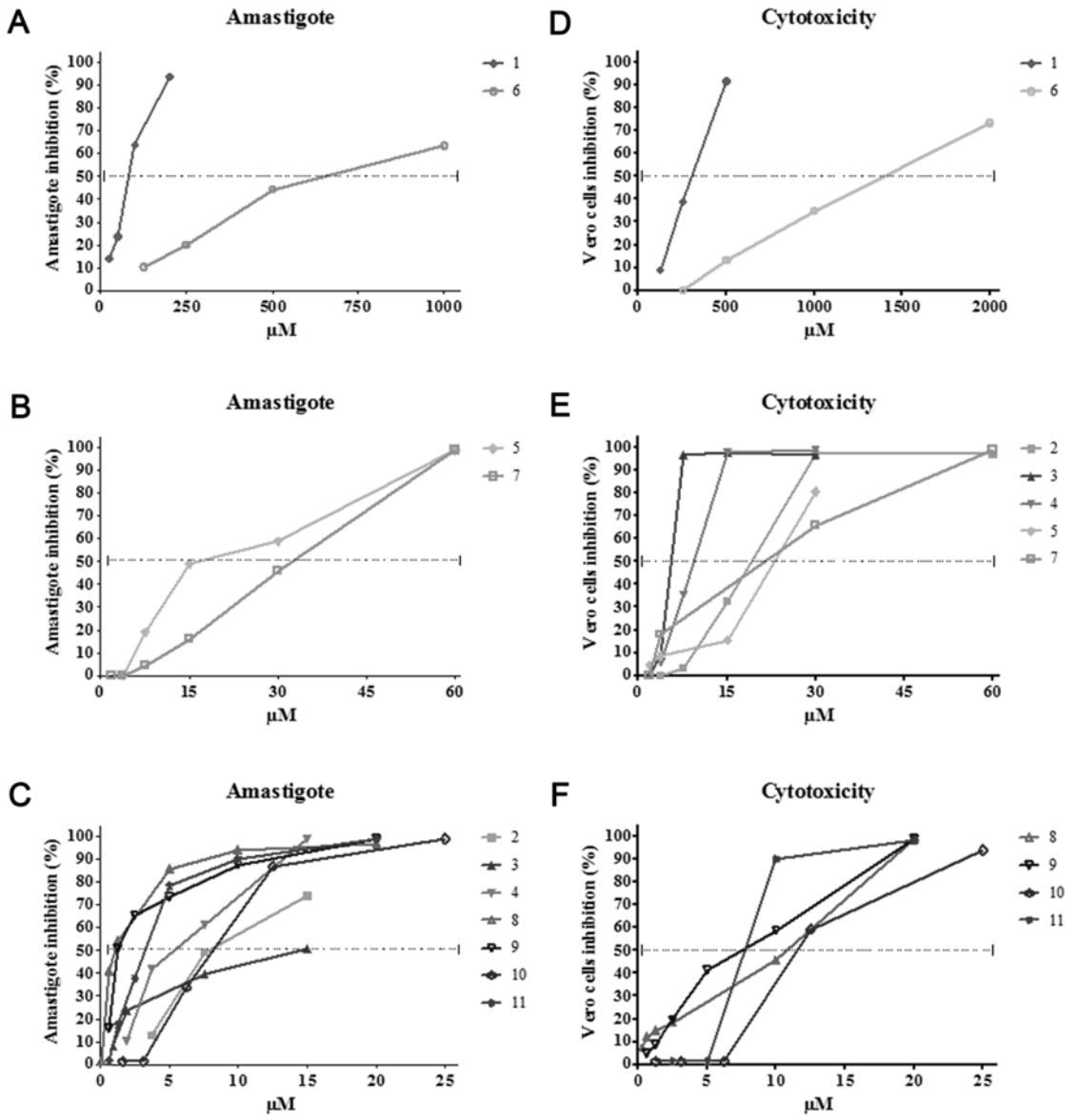


Figure 2. Dose response curves after incubation of *T. cruzi* intracellular amastigotes (A-C) and Vero cells (D-F) with different concentrations of compounds 1 to 11. Compounds were grouped according to their lower (A, D), medial (B, E) or higher (C, F) activity.

In a search for compounds with improved trypanocidal activity but with reduced cytotoxicity, a second set of quinine derivatives bearing *para*-substituted aromatic rings was synthesised. The different *para*-substituents included both electron-withdrawing (e.g. cyano- and nitro-) and electron-donating groups (e.g. methyl and methoxy). Gratifyingly, while these compounds displayed comparable activity against culture epimastigotes, they displayed noticeably higher activity against the intracellular amastigote forms (Table 2, entries 8-11 and Figure 2D-F). The IC_{50}/24 h values ranged

from 1 to 8 μM, which was within the range of our control drug benznidazole (3.1 μM). The most potent compound, which incorporated a *para*-nitro, was 83 times more effective than quinine and three times more effective than benznidazole with a submicromolar IC_{50} of 0.96 μM (entry 8). The effectiveness of **8** was further confirmed by visualising the clearance of *T. cruzi* amastigotes in infected Vero cells incubated with **8** at levels ranging from 0.078 μM to 10 μM (Figure 3). While the molecule with the most highly electron-withdrawing group was most active (entry 8), the compound with the most highly electron-donating group as almost as effective (entry 9), with no obvious relationship emerging between the nature of the substituents and biological activity. Although the effective concentration was reduced following the introduction of the *para*-substituents, the resulting compounds were still found to be toxic in mammalian cells. Nevertheless, the resulting selectivity indexes were better than that of quinine, with the most potent compound having the highest SI value (entry 8).

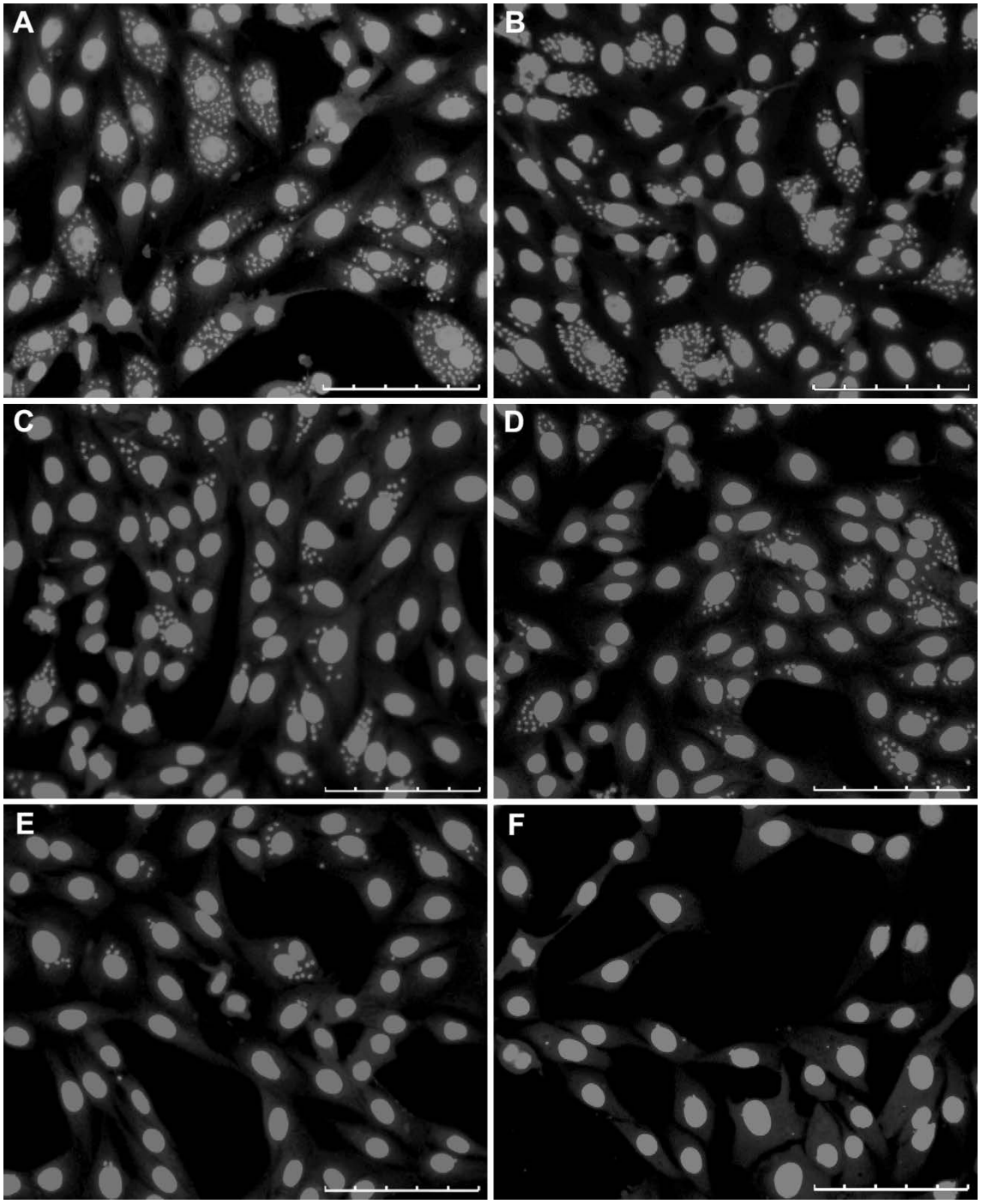


Figure 3. Detection of *T. cruzi* amastigotes in infected Vero cells with the Operetta Imaging System using Harmony software. Images from a representative experiment with **8**. Infected Vero cell cultures were incubated for 24 h with quinine derivatives and then fixed with methanol. Nuclei of host cells and intracellular amastigotes were stained with DAPI and then automatically counted. **A.** Untreated control; **B.** 0.078 µM **8**; **C**. 0.625 µM **8**; **D**. 1.25 µM **8**; **E**. 5 µM **8**; **F**. 10 µM **8**. Scale bar = 100 µm.

Since the best SI values were obtained with **8**, **9** and **11**, these were selected for further analysis by transmission electron microscopy to compare the ultrastructure of intracellular amastigotes in treated and untreated host cell cultures (Figure 4A). Incubation with quinine (reference compound) resulted in morphological alteration in the reservosomes (lysosome-related organelles), which appeared more electron-dense (Figure 4B). Interestingly, treatment with **8** resulted in no noticeable structural changes in the amastigotes (data not shown). By contrast, **9** induced a large vacuolisation of the kinetoplast, a specific region of the single mitochondrion where DNA (k-DNA) is accumulated (Figure 4C). This effect has previously been observed in *T. cruzi* treated with different drugs [28-30]. Compound **11** induced an enlargement of a vacuole close to the flagellar pocket membrane, which appears to be the contractile vacuole complex (Figure 4D). This osmo-regulation system is well characterized in *T. cruzi* epimastigotes [31, 32]. It is possible that these compounds are influencing the osmo-regulatory process of the parasite.

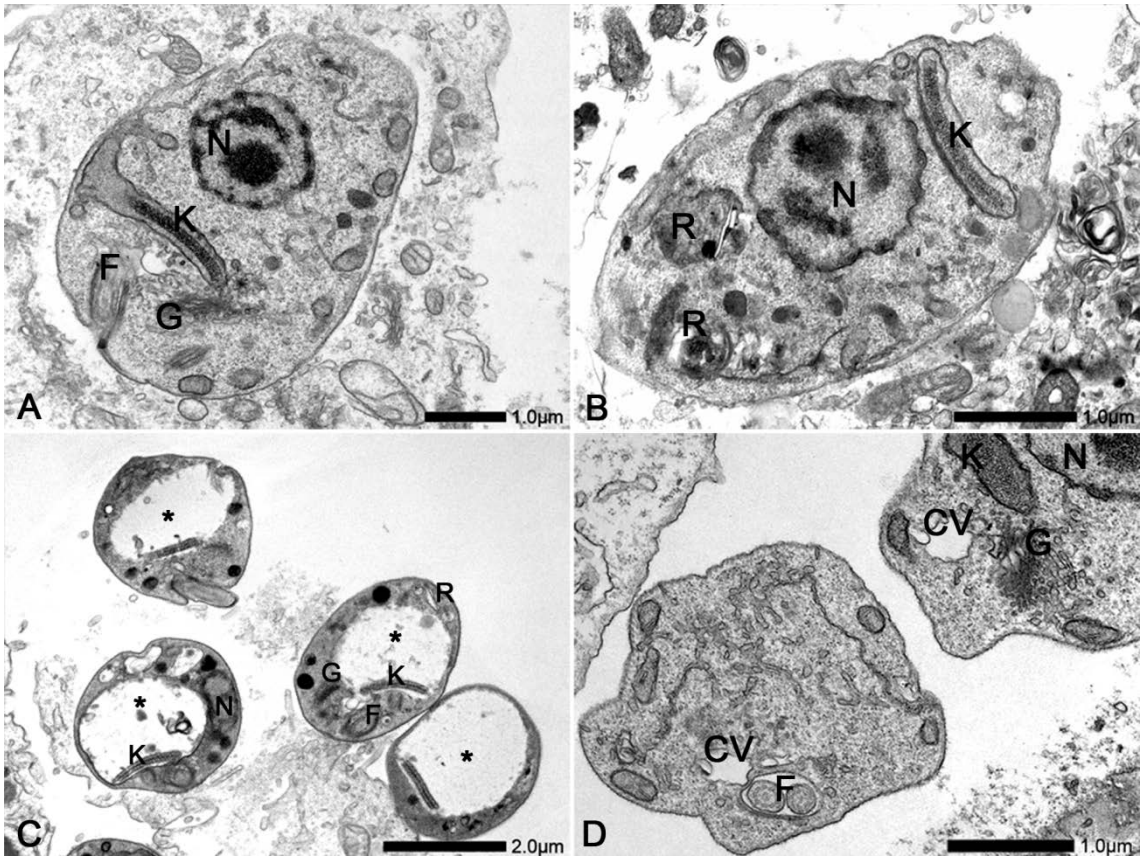


Figure 4. Ultrastructural analysis of intracellular *T. cruzi* amastigotes by transmission electron microscopy (TEM). Vero cells were incubated for 4 h with trypomastigotes (ratio 10:1) and then washed to remove non-adherent parasites. After

24 h, the infected cells were treated with the IC_{50} value of compounds and fixed for TEM. **A:** Untreated control. **B**: Quinine; reservosomes (R) lose their circular profile and appear with an electron-dense matrix. **C:** Compound **9**; the asterisks indicate enlargement of the kinetoplast region. **D:** Compound **11**; Note the enlargement of the contractile vacuole (CV), located close to the flagellar pocket. F: flagellum; G: Golgi complex; K: kinetoplast DNA; N: nucleus; R: reservosome.

Due to the large morphological alteration induced in the amastigotes kinetoplast by **9**, the effect of this compound was further analysed on cell-derived trypomastigotes. The IC_{50}/2 h was estimated as 12.5 µM. Interestingly, in incubations for 2 h, the benznidazole solution had no effect up to 1000 µM, inhibiting at most 42% of trypomastigotes. However, **9** showed high cytotoxicity against Vero cells (CC_{50}/2 h=33.33 µM; SI=2.67) (Figure 5). The ultrastructure of **9**-treated trypomastigotes was then analyzed by scanning (SEM) and transmission (TEM) electron microscopy (Figure 6). By SEM, treated parasites appeared with a round body with pointed tips. By TEM, the parasites showed the same large vacuolization in the kinetoplast, as observed with the treated intracellular amastigotes.

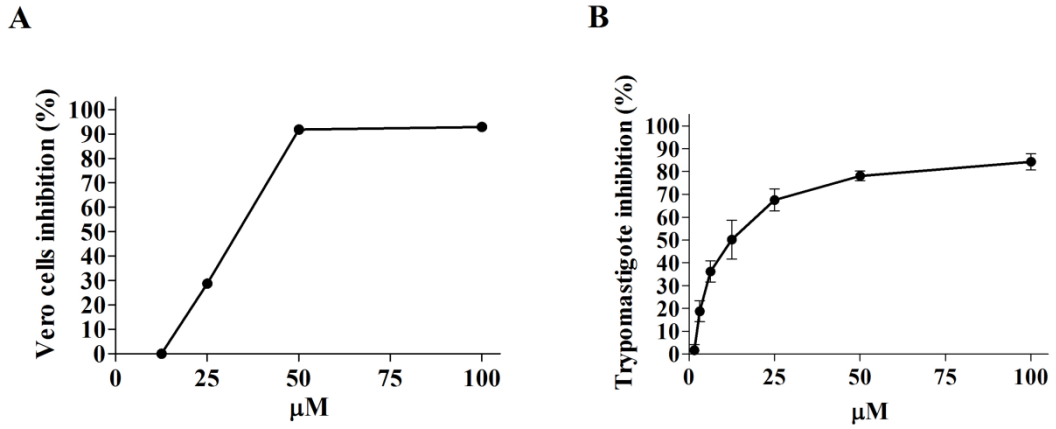


Figure 5. Determination of Vero cell cytotoxicity (CC_{50}) (A) and effect on cell-derived trypomastigotes (IC_{50}) (B) for compound 9, after incubation for 2 h at 37ºC.

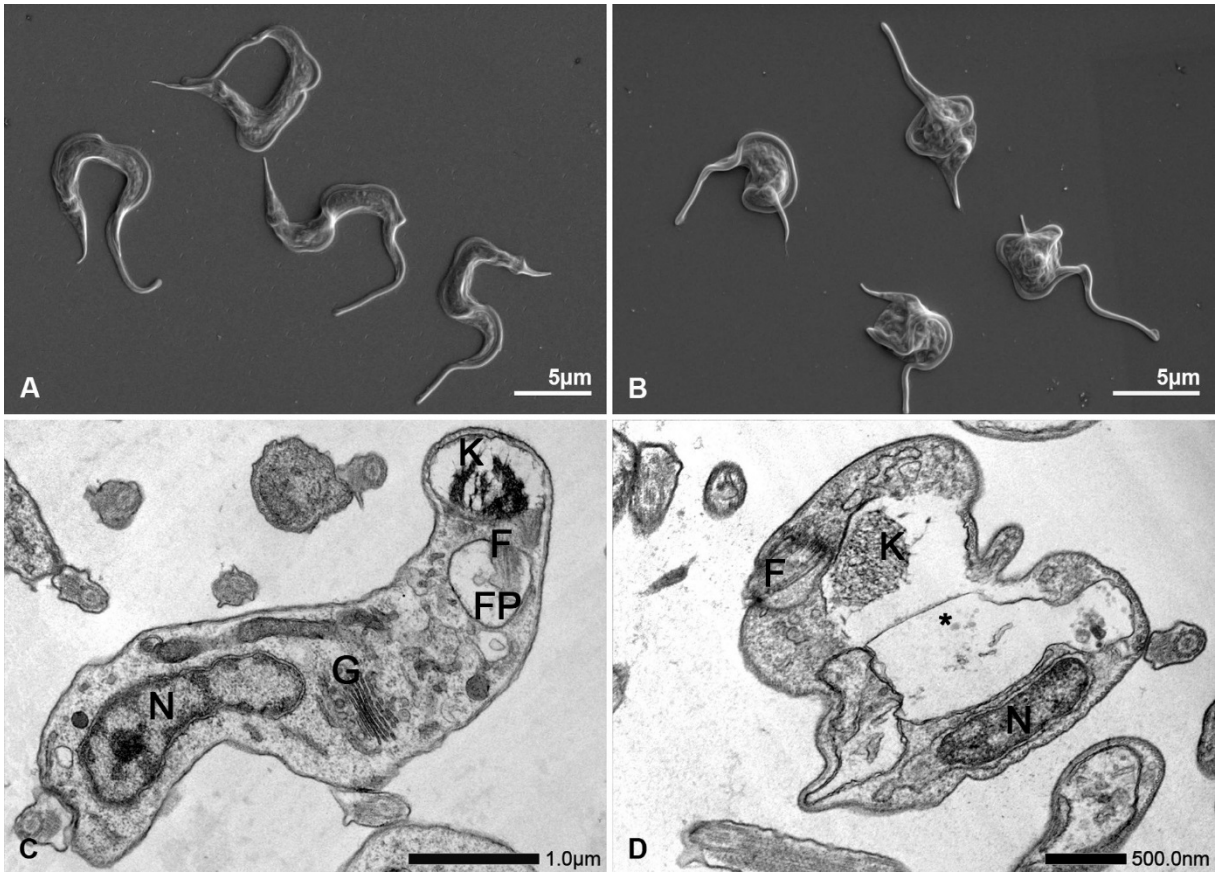


Figure 6. Scanning (A,B) and transmission (C,D) electron microscopy of cell-derived trypomastigotes incubated for 2 h with 12.5 µM compound 9. Note the rounding of the middle portion of the cell body (**B**), when compared to the typical undulating morphology of untreated parasites (**A**). Observation by transmission electron microscopy (**C, D**) shows an enlargement of the kinetoplast region (asterisk in **D**). The kinetoplast DNA (K) also appears less compact than that of control parasites (**C**). N: nucleus; G: Golgi complex; FP: flagellar pocket; K: kinetoplast.

Trypomastigotes treated with **9** were next used to infect Vero cells. It was noted that the round parasites were still able to adhere (Figure 7) and infect the host cells. The kinetoplast vacuolization of the resulting intracellular parasites was visible after 24 h (Figure 8A, B), but intracellular parasites with altered morphology were no longer visible after 48 h (Figure 8C, D). The percentage of infected cells (Table 3) was slightly reduced (about 20%), but there was a significant decrease in the number of intracellular amastigotes per cell after 48h post-infection (about 45%), when compared to untreated control cultures. Considering the infection index, the inhibition rate reached 55%. This result indicated that the treatment of trypomastigotes with **9** lead to decreased

infectivity, but the remaining parasites with normal morphology were able to maintain the infection.

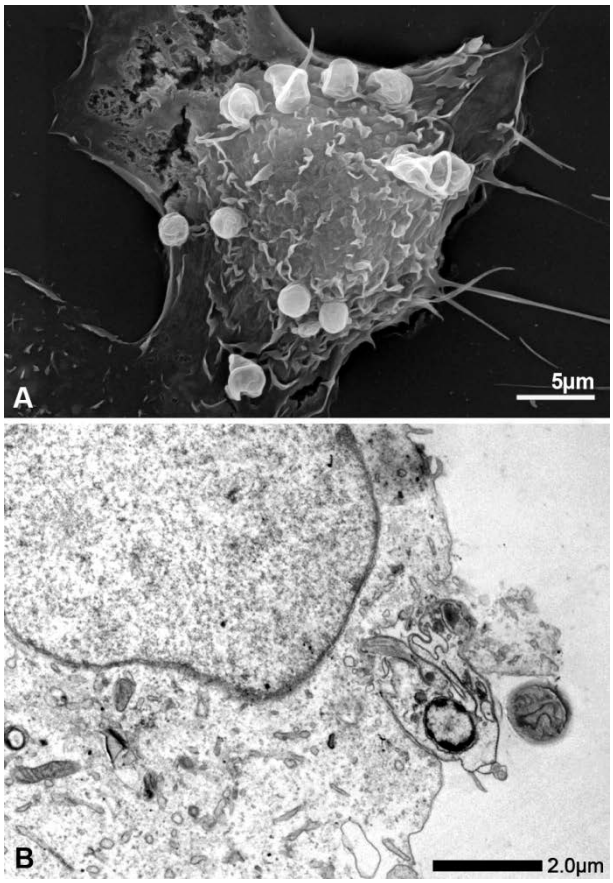


Figure 7. Scanning (A) and transmission (B) electron microscopy of Vero cells 2 h after infection. Trypomastigotes were treated with IC_{50}/2 h **9** before to cell infection. Note that the round parasites are still able to adhere (**A**) and to enter (**B**) the host cells.

Table 3. *T. cruzi* trypomastigotes were treated for 2 h with 12.5 µM (IC_{50}/2 h) **9** and then used to infect Vero cell cultures. The percentage of host cell infection and the number of intracellular amastigotes was then estimated 48 h post infection.

	% Infection	amastigotes / cell	Infectivity index
Control	20.12	1.19	23.94
9	16.31	0.66	10.76
% Inhibition	18.94	44.54	55.04

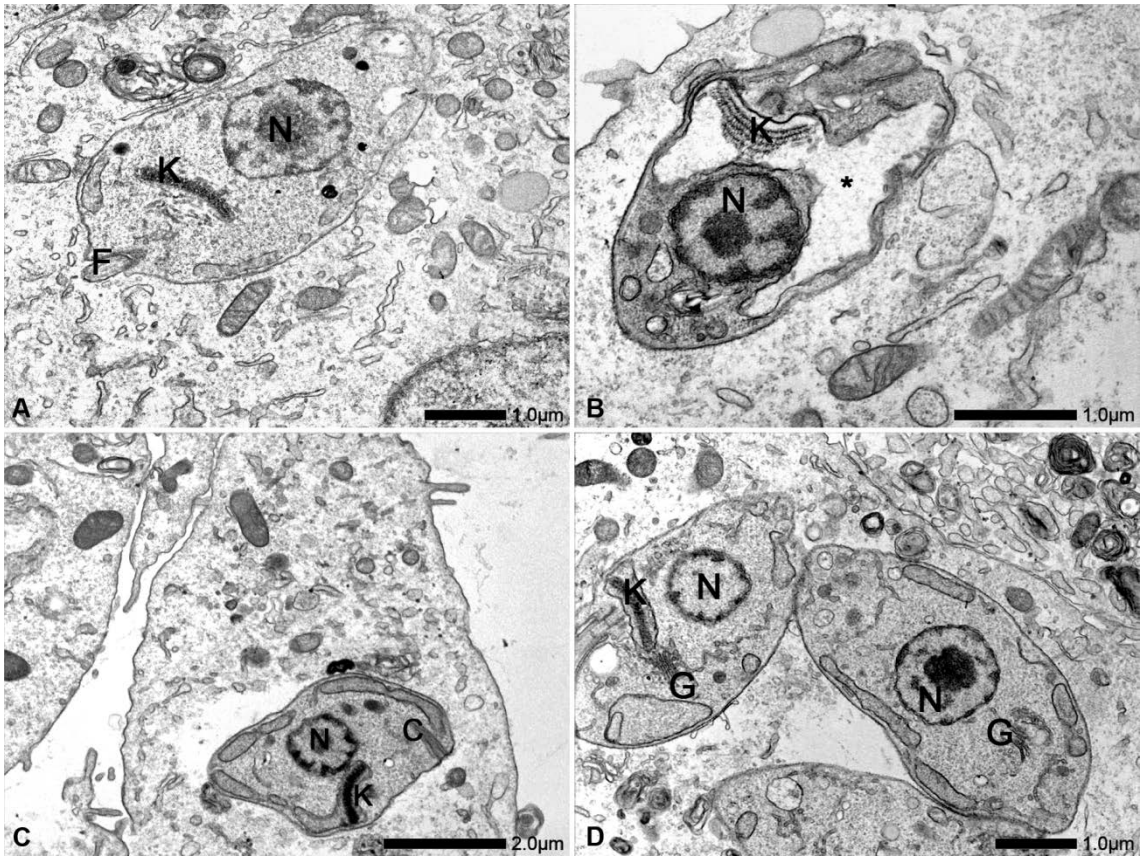


Figure 8. Transmission electron microscopy of intracellular *T. cruzi* amastigotes 24 h (A, B) and 48h post-infection (C, D). **A** and **C**: untreated controls. **B** and **D**: Infection with **9**-treated trypomastigotes. Intracellular parasites with an enlarged kinetoplast are still present 24 h post-infection (**B**), but parasites with normal morphology prevail after 48 h and maintain the infection (**D**). C: cytostome; F: flagellum; G: Golgi complex; K, kinetoplast; N: nucleus.

4. Conclusions

Our data indicates that modification of the vinyl group in quinine, in particular by the incorporation of an aromatic ring, is associated with increased trypanocidal activity against *T. cruzi*. Both the substitution pattern and choice of substituents on the ring were found to impact on potency. *Para*-substituted derivatives were discovered to be especially effective, with *para*-nitro-substituted **8** displaying a submicromolar IC_{50} which is 83 times lower than quinine and three times lower than benznidazole. These compounds were less cytotoxic than the quinine lead, with the most efficacious compound **8** having an SI value of 11.04. We have further shown that these molecules can induce significant morphological changes including large kinetoplast vacuolisation in both intracellular amastigotes and cell-derived trypomastigotes. In summary, this

work demonstrates that modification of the quinine scaffold, in particular by incorporation of an aryl ring onto the vinyl group, affords compounds with high trypanocidal activity against *T. cruzi*. Such an approach offers significant potential for the development of new drugs for the treatment of Chagas disease.

5. Future Perspective

Many millions of people worldwide are infected with *T. cruzi*, the causative agent of Chagas disease. In spite of this, Chagas remains a neglected disease, with the main treatments having been developed many decades ago. Long term use of these therapies is associated with severe side-effects and instances of treatment failure are becoming increasingly common. Additionally, while Chagas disease was once largely confined to Latin America, it has become more widespread in recent years due to increased population movements. Indeed, some have suggested that an increase in global temperatures due to climate change may lead to even greater global prevalence. These factors underline the importance of developing new, safe and efficacious alternatives. Quinine has long been used as an anti-parasitic compound, but had fallen out of favour with the introduction of cheaper and more effective aminoquinolines such as chloroquine. However, increased parasite resistance has resulted in renewed interest in quinine, both as a standalone medication or in combination with other drugs with complemtary modes of action. This interest is also partly due to the versatile nature of the quinine molecule which offers multiple opportunities for further manipulation. Furthermore, advances in synthetic chemistry, such as palladium-catalysed carbon-carbon bond formation, have facilitated the modification of the quinine scaffold in novel ways. This combination of “old molecules” with “new chemistry” opens up new avenues for the development of effective leads in treating neglected, parasitic diseases.

6. Acknowledgements

The authors thank the Program for Technological Development in Tools for Health-PDTIS FIOCRUZ for the use of its facilities (Platform RPT07C – Confocal and Electron Microscopy-PR). H.G. wishes to thank the Irish Research Council for funding.

7. Financial & competing interests disclosure

This work was supported by the Irish Research Council [Government of Ireland PhD Scholarship GOIPG/2013/113], Conselho Nacional de Desenvolvimento Científico e

Tecnológico (CNPq) and Fundação Oswaldo Cruz (Fiocruz). The authors have no other relevant affiliations or financial involvement with any organization or entity with a financial interest in or financial conflict with the subject matter or materials discussed in the manuscript.

Executive Summary:

-Novel, aryl-substituted analogues of quinine display significantly increased trypanocidal activity against *T. cruzi*.

-*Para*-substituted aromatic analogues are especially potent, with the *para*-nitro-derivative displaying a submicromolar IC_{50} which is three times lower than benznidazole.

-Compounds with either electron-donating and electron-withdrawing substituents in the *para*-position are equally effective.

-Analysis by transmission electron microscopy analysis confirmed that that these compounds induced a marked vacuolisation of the kinetoplast of *T. cruzi* intracellular amastigotes and cell-derived trypomastigotes.

References:

1. Bern C. Chagas' Disease*. N. Engl. J. Med.* 373 456-466 (2015).

** Provides an up-to-date overview of the impact and treatment of Chagas disease.

2. Tempone AG, Sartorelli P, Mady C, Fernandes F. Natural products to anti-trypanosomal drugs: an overview of new drug prototypes for American Trypanosomiasis*. Cardiovasc. Hematol. Agents Med. Chem.* 5 222-235 (2007).
3. Coura JR, Borges-Pereira J. Chronic phase of Chagas disease: why should it be treated? A comprehensive review. *Mem. Inst. Oswaldo Cruz* 106(6), 641-645 (2011).
4. Castro JA, Diaz De Toranzo EG. Toxic effects of nifurtimox and benznidazole, two drugs used against American trypanosomiasis (Chagas' disease)*. Biomed. Environ. Sci.* 1(1), 19-33 (1988).
5. Pinazoa M-J, Guerrerob L, Posada E, Rodríguez E, Soy D, Gascona J. Benznidazole-Related Adverse Drug Reactions and Their Relationship to Serum Drug Concentrations in Patients with Chronic Chagas Disease*. Antimicrob. Agents Chemother.* 57(1), 390-395 (2013).
6. Meshnick S, Dobson M. In: *Antimalarial Chemotherapy Mechanism of Action Resistance and New Directions in Drug Discovery*, Rosenthal P (Ed.^(Eds).Humana Totowa, NJ 15-26 (2001).
7. Vandekerckhove S, D'hooghe M. Quinoline-based antimalarial hybrid compounds*. Bioorg. Med. Chem.* 23 5098-5119 (2015).
8. Achan J, Talisuna AO, Erhart A *et al*. Quinine, an old anti-malarial drug in a modern world: role in the treatment of malaria*. Malar. J.* 10 144 (2011).
9. Merschjohann K, Sporer F, Steverding D, Wink M. *In Vitro* Effect of Alkaloids on Bloodstream Forms of *Trypanosoma brucei* and *T. congolense. Planta Med.* 67(7), 623-627 (2001).

10. Ruiz-Mesia L, Ruiz-Mesia W, Reina M *et al*. Bioactive *Cinchona* Alkaloids from *Remijia peruviana*. *J. Agric. Food Chem.* 53(6), 1921-1926 (2005).
11. Sepúlveda-Boza S, Cassels BK. Plant metabolites active against *Trypanosoma cruzi*. *Planta Med.* 62(2), 98-105 (1996).
12. Alumasa JN, Gorka AP, Casablanca LB, Comstock E, De Dios AC, Roepe PD. Investigating the activity of quinine analogues vs. chloroquine resistant *Plasmodium falciparum. J. Inorg. Biochem.* 105 467-475 (2011).
13. Jones RA, Panda SS, Hall CD. Quinine conjugates and quinine analogues as potential antimalarial agents*. Eur. J. Med. Chem.* 97 335-355 (2015).
14. Foley M, Tilley L. Quinoline antimalarials: mechanisms of action and resistance and prospects for new agents*. Pharmacol. Ther.* 79 55-87 (1998).
15. Arrington MP, Bennani YL, Gobel T, Walsh P, Zhao SH, Sharpless KB. Modified cinchona alkaloid ligands: Improved selectivities in the osmium tetroxide catalyzed asymmetric dihydroxylation (AD) of terminal olefins*. Tetrahedron Lett.* 34 7375-7378 (1993).
16. Fache F, Piva O. New perfluoroalkylated cinchona derivatives: synthesis and use in base-catalysed Diels–Alder reactions*. Tetrahedron Lett.* 42(33), 5655-5657 (2001).
17. Merschaert A, Delbeke P, Daloze D, Dive G. The rational design of modified Cinchona alkaloid catalysts. Application to a new asymmetric synthesis of chiral chromanes*. Tetrahedron Lett.* 45 4697-4701 (2004).
18. Ma B, Parkinson JL, Castle SL, 2007, 2083. Novel Cinchona alkaloid derived ammonium salts as catalysts for the asymmetric synthesis of beta-hydroxy alpha-amino acids via aldol reactions*. Tetrahedron Lett.* 48 2083-2086 (2007).
19. O'Reilly K, Gupta MK, Gandhi H *et al*. Cinchona-catalysed, enantioselective synthesis of β-peroxycarboxylic acids, β-peroxyesters and β-peroxyalcohols*. Curr. Org. Chem.* 20 1-6 (2016).
20. Dinio T, Gorka AP, McGinniss A, Roepe PD, Morgan JB. Investigating the activity of quinine analogues versus chloroquine resistant *Plasmodium falciparum. Bioorg. Med. Chem.* 20 3292-3297 (2012).

*Demonstrates the effectiveness of modifying the quinine scaffold as a route to novel anti-malarial compounds.

21. Bhattacharjee AK, Hartell MG, Nichols DA *et al*. Structure-activity relationship study of antimalarial indolo [2,1-b]quinazoline-6,12-diones (tryptanthrins). Three dimensional pharmacophore modeling and identification of new antimalarial candidates*. Eur. J. Med. Chem.* 39 59-67 (2004).
22. Beletskaya IP, Cheprakov AV. The Heck Reaction as a Sharpening Stone of Palladium Catalysis*. Chem. Rev.* 100(8), 3009-3066 (2000).
23. Denizot F, Lang R. Rapid colorometric assay for cell growth and survival. Modifications to the tetrazolium dye procedure giving improved sensitivity and reliability*. J. Immunol. Meth.* 89(271-277), (1986).
24. Sykes ML, Avery VM. Development and application of a sensitive, phenotypic, high-throughput image-based assay to identify compound activity against *Trypanosoma cruzi* amastigotes*. Int. J. Parasitol. Drugs Drug. Resist.* 5 215-228 (2015).

*Describes Operetta, an image-based system that determines the effect of compounds against *T. cruzi* amastigotes, but is also capable of estimating the toxicity of compounds on host cells.

25. Fonseca-Berzal C, Rojas Ruiz FA, Escario JA, Kouznetsov VV, Gómez-Barrio A. *In vitro* phenotypic screening of 7-chloro-4-amino(oxy)quinoline derivatives as putative anti-*Trypanosoma cruzi* agents*. Bioorg. Med. Chem. Lett.* (24), 1209–1213 (2014).
26. Purser S, Moore PR, Swallow S, Gouverneur V. Fluorine in medicinal chemistry*. Chem. Soc. Rev.* 37(2), 320-330 (2008).

27. Villamizar LH, Cardoso MG, Andrade J, Teixeira ML, Soares MJ. Linalool, a Piper aduncum essential oil component, has selective activity against *Trypanosoma cruzi* trypomastigote forms at 4°C*. Mem. Inst. Oswaldo Cruz* 112 131-139 (2017).
28. Lorente SO, Rodrigues JC, C. JJ *et al*. Novel azasterols as potential agents for treatment of leishmaniasis and trypanosomiasis*. Antimicrob. Agents Chemother.* 48 2937-2950 (2004).
29. Britta EA, Scariot DB, Falzirolli H *et al*. 4-Nitrobenzaldehyde thiosemicarbazone: a new compound derived from S-(-) -limonene that induces mitochondrial alterations in epimastigotes and trypomastigotes of *Trypanosoma cruzi. Parasitology* 142 978-988 (2015).
30. Volpato H, Desoti VC, Valdez RH *et al*. Mitochondrial dysfunction induced by *N*-butyl-1-(4-dimethylamino)phenyl-1,2,3,4-tetrahydro-β-carboline-3-carboxamide is required for cell death of *Trypanosoma cruzi. PLoS ONE* 10 e0130652 (2015).
31. Rohloff P, Docampo R. A contractile vacuole complex is involved in osmoregulation in *Trypanosoma cruzi. Exp. Parasitol.* 118 17-24 (2008).
32. Docampo R, Jimenez V, Lander N, Li ZH, Niyogi S. New Insights into the roles of acidocalcisomes and the contractile vacuole complex in osmoregulation in protists*. Int. Rev. Cell Mol. Biol.* 305 69-113 (2013).